PAPER • **OPEN ACCESS**

Calibration Mechanism Design and Stiffness Analysis

To cite this article: Siyu Xia *et al* 2019 *IOP Conf. Ser.: Mater. Sci. Eng.* **520** 012014

View the article online for updates and enhancements.

IOP ebooks™

Bringing you innovative digital publishing with leading voices to create your essential collection of books in STEM research.

Start exploring the collection - download the first chapter of every title for free.

This content was downloaded from IP address 123.169.115.99 on 19/09/2019 at 18:46

IOP Conf. Series: Materials Science and Engineering **520** (2019) 012014 doi:10.1088/1757-899X/520/1/012014

Calibration Mechanism Design and Stiffness Analysis

Siyu Xia[1], Jinfeng Shi[1], Guorui Ren[1] and Chuang Li[1,a]

[1] Xi'an Institute of Optics and Precision Mechanics, Chinese Academy of Sciences, 17 Xinxi Road.

[a] Corresponding author: lichuang@opt.ac.cn; Tel: 13991368272

Abstract. According to the optical requirements of a space camera, a calibration mechanism in the form of a worm gear driven cantilever beam is designed, and a stop is added at the cantilever beam's end for limiting its amplitude. A detailed finite element model considering the clearance between moving parts in the mechanism and the preload of bearing is established using MSC.Patran & Nastran. By comparing the vibration test and analysis results, the stiffness and the dynamic environment adaptability of the mechanism is investigated and the first-order resonant frequency of the calibration mechanism is much larger than 100Hz which is high enough for the telescope's structure. Finally, the result shows that the error between the analysis result and the test data is within 10%, and it is verified that the calibration mechanism scheme has higher stiffness.

1. Introduction

The on-orbit calibration of space cameras is the guarantee for long-term stable observation targets[1-2]. The on-track calibration of a space camera design uses the traditional built-in lamp calibration method of "LED light source + diffuse reflector". According to the optical design scheme, the diffuse reflection plate is located between the lens of the optical path and the LED lamp. As shown in Fig. 1. It needs to be turned in and out. When it is transferred into the optical path it works as a calibration. It also has the function of a shutter. Since the diffuse reflector has a small distance from the optical elements on both sides and undergoes a harsh mechanical environment during the launching process, the moving structure is required to have a high rigidity.

In the process of machining and assembly of the worm gear, the meshing backlash is inevitable, and the no-load backlash represents the inherent error of the drive combination. In the reference [3], the analysis result is higher than the test result without considering the worm gear backlash. However, the rigidity of the worm gear mechanism increases after the filler is added to eliminate the backlash, so the backlash of the worm gear has a great influence on the structural rigidity. The backlash of the worm gear can cause collision and impact between the contact surfaces of the tooth surfaces during the environmental test, thereby affecting the structural rigidity. In order to quantitatively study the influence of this contact gap, from Hertz's theory of contact problems in 1882, many practical numerical calculations of contact problems have emerged [4-5]. The formula for calculating the stiffness of angular contact ball bearings with preload is introduced in [6].

Content from this work may be used under the terms of the Creative Commons Attribution 3.0 licence. Any further distribution of this work must maintain attribution to the author(s) and the title of the work, journal citation and DOI.
Published under licence by IOP Publishing Ltd

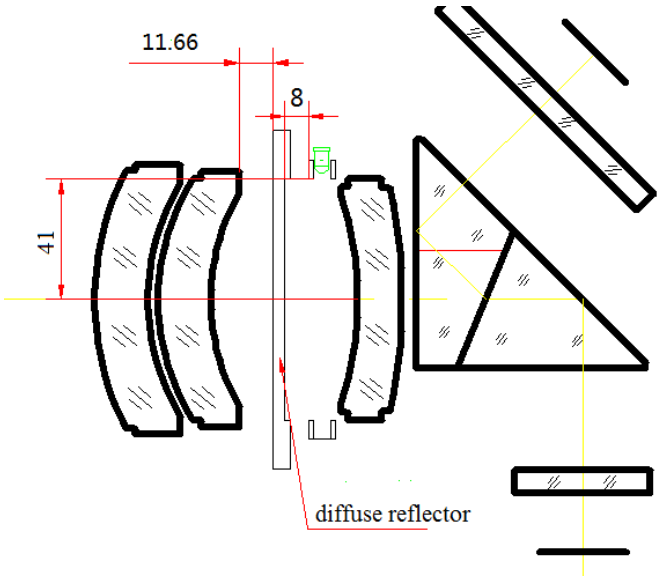

Figure 1. The relationship between optical components

The structural design of the calibration mechanism is given in this paper, and the mechanical properties of the whole mechanism are modeled and analyzed by finite element using gap theory. The structural design is improved through experiments, which effectively improves the rigidity of the mechanism. This experience provides a type of design for the future space rotation mechanism to be based on.

2. Calibration Assembly design

According to the requirements of the calibration system, the calibration mechanism needs to remain locked during launch. Due to the self-locking characteristics of the worm gear and the stall torque generated by the stepper motor, the calibration is actuated by the stepper motor and the worm gear. Because of the limited space, angular contact ball bearings are mounted back to back on both sides rather the same side of the worm wheel to increase its rigidity. In order to ensure normal operation in the space environment, all of the moving parts in the calibration mechanism are lubricated with MoS2 to avoid the phenomenon of "cold welding".

The diffuser plate of the calibration mechanism is located in the middle of the optical component with a relatively close distance, and the diameter of the calibration plate is relatively large, so that the end of the diffuser plate frame of the actuator of the calibration mechanism forms a long cantilever beam. Several designs are proposed and optimized in the reference [7] to reduce the deformation of the vibration and improve the stiffness of the system. The mechanical environment of the launch section is harsh. In order to prevent the cantilever beam from undergoing large deformation during the vibration process and colliding with the lens system on both sides, a stop limit is added at the end of the diffuse reflector frame. It also works as a hard stop for the mechanism.

The latest design of the calibration mechanism is composed of a fixed PTFE diffuse reflector of 82mm diameter, a stepper motor with 1.8 °per step and a potentiometer, worm gear mechanism with a reduction ratio of 1:50, an end stop, flexible couplings avoid motion jams caused by machining and installation errors, angular contact ball bearings which can improve shaft stiffness and all necessary interfaces and housing.

The mechanism's total mass is about 1.5kg. The detailed model of the overall calibration mechanism is shown in Figure 2.

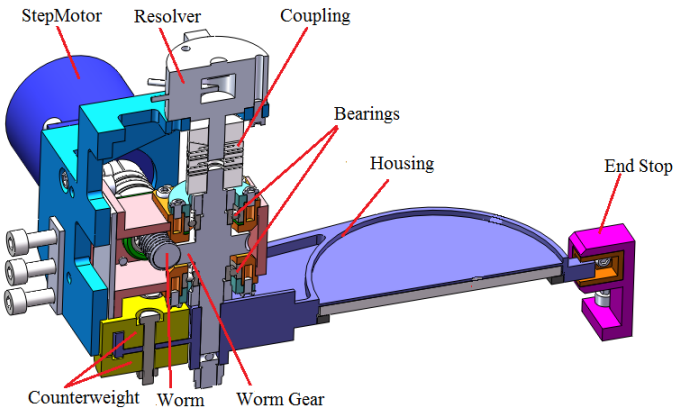

Figure 2. Detailed structure of the calibration mechanism

3. Finite Element and Modal Reduction

The calibration mechanism mainly includes worm gears, angular contact ball bearings, flexible couplings, stoppers and brackets. Different parts with different characteristics are modelled by different units to obtain results conform to the actual condition.

The solution to the contact problem requires an accurate determination of the contact state and the application of the correct contact conditions. The contact state is generally divided into three types: a separated state, a bonded contact state, and a sliding contact state. In either form, after the structure is discretized, the following contact conditions are always met between the pairs of contact points, and finally the contact conditions of the discretized form are obtained:

Normal:

$$B_n U + D_0 \geq 0 \tag{1}$$

Tangential:

$$B_t \left(U\left(t+\Delta t\right) - U\left(t\right) \right) = 0 \tag{2}$$

$U\left(t\right)$ represents the node displacement vector at time *t*, B_n , B_t is the contact constraint matrix, and D_0 is the initial normal gap.

The motion of any structural system can be expressed as a set of equilibrium equations for internal, external and inertial forces:

$$\left[M\right] \left\{\ddot{U}\right\} + \left[C\right] \left\{\dot{U}\right\} + \left[K\right] \left\{U\right\} = \left\{P\left(t\right)\right\} + \left\{N\right\} + \left\{Q\right\} \tag{3}$$

Where [*M*]: mass matrix; [*C*]: damping matrix; [*K*]: stiffness matrix; {*P(t)*}: external force function vector; {*N*}: associated nonlinear external force term vector; {*Q*}: boundary constraint reaction vector; $\{U\}$: displacement vector; $\{\dot{U}\}$ velocity vector; $\{\ddot{U}\}$ acceleration vector.

After the system design is completed, the mass matrix [*M*] is constant. When the gap exists, in the state where the two objects are not in contact, the stiffness of the unit between the pair of contact points is close to zero. After reaching the area where the two objects contact, the stiffness of the unit tends to the stiffness of the contacted object, it means at this time the unit's stiffness matrix [*K*] changes with the displacement vector {*U*}, and the damping matrix [*C*] also changes accordingly, so the system becomes a nonlinear system with variable stiffness and variable damping [8-10].

The contact between the worm and the worm gear is in a separated state without external force interference, that is, the contact force is zero, and the contact surface is in a free motion state. The node pairs are selected in the contact areas of the two parts to simulate their contact stiffness using springs.

The angular contact ball bearing of the mechanism is directly connected with the structure of the worm wheel and the reduction gear box. The rigidity of the ball contact bearing has a great influence

on the dynamic characteristics of the system. Under the axial preload force, the axial stiffness of the angular contact ball bearing is:

$$K_t = 6.86\left(Z^2 D_w \sin^5 \alpha_0\right)^{1/3} F_0^{1/3} \tag{4}$$

The radial stiffness is:

$$K_r = 1.7164 D_w^{1/3} Z^{2/3} \frac{\cos^2 \alpha_0}{\sin^{1/3} \alpha_0} F_0^{1/3} \tag{5}$$

In the above two formulas (4) and (5), F_0 is the axial preload (N), Z is the number of rigid balls in a single set of bearings, D_w is the diameter of the rigid ball (mm), and α_0 is the initial contact angle(°).

When the preload is too large, the torque required to drive the worm wheel is large, the wear on the motor and the coupling is large, the system's life is reduced; when the preload is too small, the system's stiffness is low, the mechanical properties cannot be met, and When the shaft system vibrates, the potentiometer will generate large sway and the accuracy will decrease. When the axial preload force is 7N, the axial stiffness is 13400N/mm, and the radial stiffness is 46780N/mm.

The flexible coupling is an important component of the transmission on the shafting system. The selection of the design has a great influence on the rigidity of the mechanism. In order to better simulate the real state, the flexible part needs to be refined as show in figure 3.

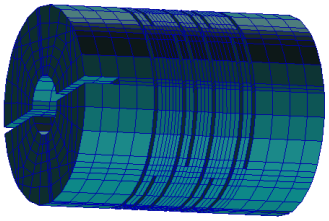

Figure 3. FEM of the Flexible coupling

For the stopper at the end of the diffuse plate frame, under the initial vibration condition, there is a certain gap between the block and the frame, and the end of the frame will collide with the polyimide on the block to generate an impact during the vibration. This contact pair is a separate contact, and the contact deformation between the two is relatively small, and is simulated by the spring unit with small stiffness.

The whole mechanism is fixed on the telescope through the four mounting points on the leftmost plane while the end stop mounted on the other side of the telescope.

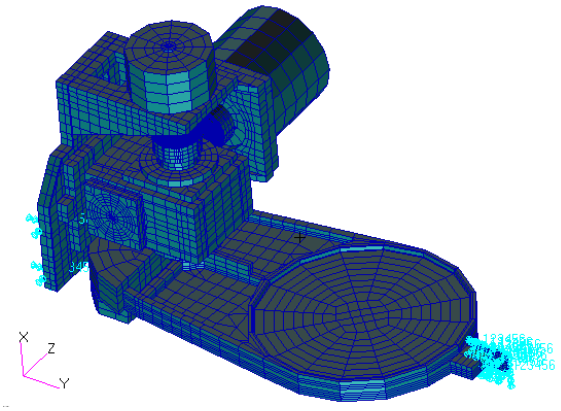

Figure 4. The mesh partition of calibration mechanism

The modeling of the structural components of the calibration mechanism mainly uses the entities (Hex8 and Wedge6). In the final model, there are 34,685 nodes and 23,070 cells. The model is shown in Figure 4. The material parameter tables used in the model are shown in Table 1 below.

Table 1. Material parameter in the model

Material	Young's modulus (GPa)	Poisson's ratio	Density (Kg/m^3)	Components
TC4	109	0.34	4430	Support
Aluminum alloy	78	0.33	2700	Worm gear, housing
45# steel	205	0.29	7850	Worm
PTFE	3	0.35	1390	Diffuse reflector
Copper	110	0.33	8930	Counterweight

4. Vibration Experiment and Analysis

In order to verify the correctness of the results of the FEM analysis and the response of the structure in the mechanical environment, the actual product was mounted on the jigs for mechanical testing. In Fig. 5, the state in which the X direction is subjected to the mechanical test is performed, and in the other two directions, it is only necessary to change the mounting direction of the tooling and the test stand.

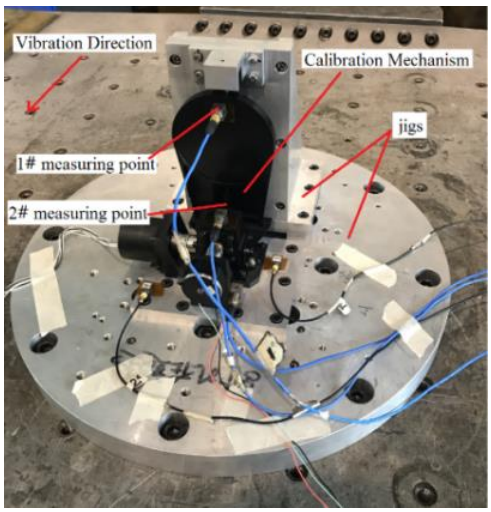

Figure 5. X-direction test

The mechanical test conditions are 0.5g characteristic sweep in 5~500Hz in 3 directions, and sinusoidal and random vibration tests in 3 directions. Through the axial low-level sine sweep test, the three-way measured fundamental frequency of the product is obtained. Table 2 gives the results of the modal analysis and the three-direction test sweep curves at the 1# measurement point.

It can be seen from Table 2 that the fundamental frequencies in the three directions are the rotation around the X, Y, and Z axes of the diffuse reflector frame, and the first-order fundamental frequency and analysis results of the characteristic sweep curves of the 1# measuring points are extracted. The fundamental frequency of the direction is summarized as shown in Table 3 below.

Table 3 shows that the fundamental frequency of the calibration mechanism is 143Hz, which is much higher than the demands of 100Hz, and the analysis results of the first-order fundamental frequency of X and Y are slightly different from the experimental results, while the results of the Z-direction first-order fundamental frequency analysis differ from the experimental results by 13 Hz, but the difference is still within 10%, and the analysis result is proven to be accurate.

Table 2. modal analysis results and experimental sweep frequency curves

	Modal analysis result	Test result (sweep curve)
X	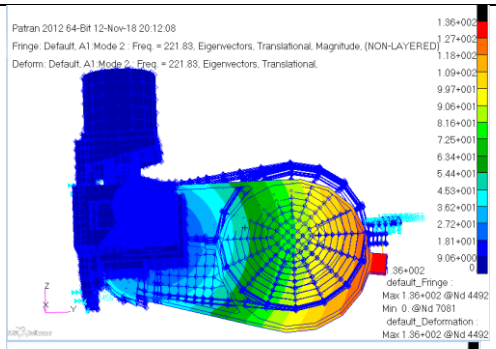	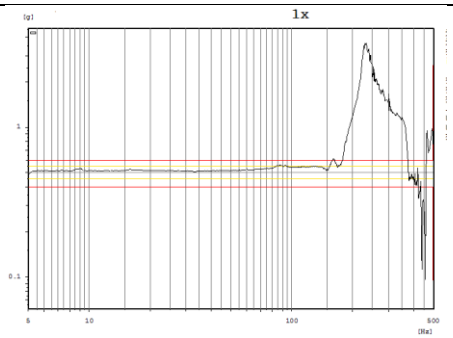
Y	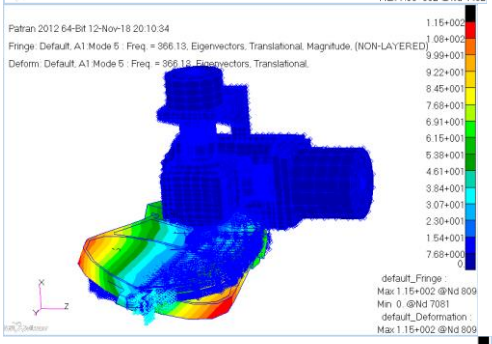	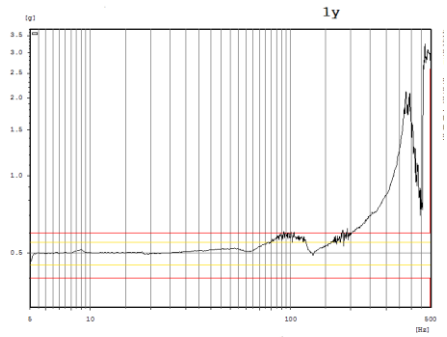
Z	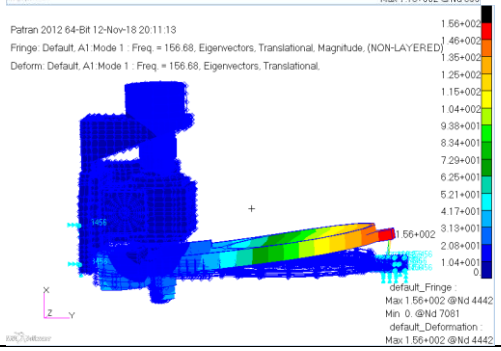	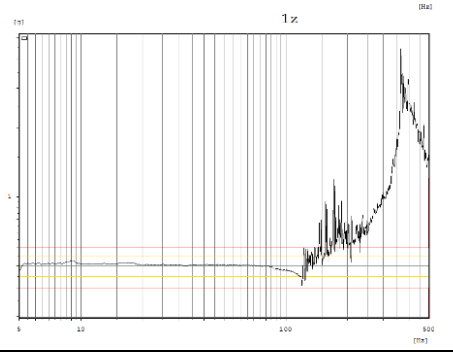

Table 3. resonant frequency

Direction	X	Y	Z
Measured (Hz)	220	376	143
Analysis result (Hz)	222	366	156
Difference (%)	0.9	2.7	9.09

5. Conclusions

According to the positional characteristics of the diffuse reflector in the optical path and the severe launching mechanical conditions, a calibration mechanism with an amplitude limit is designed. The results of finite element analysis and mechanical tests show that the first-order resonant frequency of the calibration mechanism is much larger than 100Hz, the shafting design of the calibration mechanism is reasonable and has high rigidity, which can meet the requirements of mechanical vibration. The difference between the analysis results and the test results is small, indicating that the simulation unit considering the mechanism clearance can provide a reference for the similar stiffness analysis of the rotating mechanism in the future.

References

[1] Gu X, Tian G, Yu T, Li X, Gao H, Xie Y, [Space Optical Remote Sensor Radiometric Calibration Principle and Method], Science Publishers, Beijing, 172-177 (2013)
[2] Adrian M G, Ulrich L, Alex Z and Manuel G, A Contamination Control Cover for the Mid Infrared Instrument of the James Webb Space Telescope, *Proc. SPIE 7018, 70184L1-70184L8 (2008).*
[3] W. Yongbin. Harbin Institute of Technology. (2009)
[4] H Herz, J Re. Angew Math. **92**:156-171(1882)
[5] L Shu, L Jingbo, F Ehua. J Eng Mech-ASCE, **12**:14-28(1999)
[6] Z Jingxu. Optics Precis Eng. **2**. 73-77(1996)
[7] C Yaqin, L Chuang, X Siyu, Z Peifeng, L Wang. *Proc. SPIE 10339, Pacific Rim Laser Damage 2017: Optical Materials for High-Power Lasers, 103391S*
[8] J T Stadter, R O Weiss. Computers &Structures. **10**:867-873(1979).
[9] L Zhaohui, W Zhongsu, H Qinglong, Y Liang. Chin J Sci Inst. **11**:2535-2541(2013)
[10] X Shifu, C Bin, D. Qiang, M Jun. J Dyn Control. **12**,35-40(2003)